Precise Characterization of the B ($^1/_2$) and C ($^3/_2$) States of XeF from a Deperturbation Analysis of the B → X Spectrum of ^{136}XeF†

Patricia C. Tellinghuisen and Joel Tellinghuisen*

Department of Chemistry, Vanderbilt University, Nashville, Tennessee 37235

Received: December 28, 2001; In Final Form: March 17, 2002

The B ($^1/_2$) and C ($^3/_2$) ion-pair excited states of XeF are coupled by the rotational Hamiltonian, producing perturbations in the rotational structure of B → X($^2\Sigma^+$) transitions involving v' levels <5. Five v' -v'' bands in the B → X emission spectrum of the single isotopomer ^{136}Xe^{19}F are analyzed by a deperturbation model to yield improved spectroscopic parameters (cm^{-1}) for the low-v regions of the B and C states: For B, ω_e = 308.09, $\omega_e x_e$ = 1.480, B_e = 0.145 29, and α_e = 0.000 675; for C, ω_e = 345.1, $\omega_e x_e$ = 2.10, B_e = 0.165 42, and α_e = 0.001 48. The C state lies 797 cm^{-1} below the B state, with R_e = 2.473 Å. The electronic perturbative coupling element for B−C interactions is 1.632, which is 6% below the simple Hund's case c-based prediction ($\sqrt{3}$) and just 3% greater than an estimate obtained from a more elaborate case a approach.

Introduction

Although XeF was identified spectroscopically as early as 1963,[1−3] it first aroused real interest in the heady times surrounding the discovery of the rare gas halide (RgX) lasers in 1975. Velazco and Setser reported UV emission for all four XeX species from low-pressure flowing afterglow reactions of halogen-bearing compounds with electronically excited Xe atoms;[4] and the XeF laser became the second RgX laser to be announced[5] (after XeBr[6]). The lasing transitions were labeled B−X and were quickly understood as charge-transfer transitions from a bound ion-pair excited state to the essentially unbound ground state.[7] This picture (see Figure 1) was corroborated by more detailed theoretical computations.[8−10] Yet XeF was unique among the RgX species, in that its emission spectrum at high pressures exhibited rich fine structure that could not possibly arise from the bound-free transitions expected.[11,12] To the contrary, the X state had to be bound by much more than predicted for only van der Waals attractive forces.[13] Not surprisingly, XeF became the focus of much attention by molecular spectroscopists.

The first successful vibrational analysis of the B−X system was reported from our laboratory, working in collaboration with a group from Sandia.[14] Through a further collaboration with Setser's group and John Coxon, we extended this work to include the rotational analysis of a single $v'-v''$ emission band (1−2), for which by happenstance the isotopic shifts in the various XeF isotopomers canceled out, leaving well-resolved rotational structure.[15,16] The latter work also corroborated and refined an earlier analysis of the higher energy D−X system, also from Setser's group and Coxon.[17] The vibrational analysis of the B−X system was confirmed by Smith and Kobrinsky[18] in a flash-photolysis transient absorption experiment; and a high-resolution nozzle-jet study by Monts et al.[19] corroborated and extended the rotational analysis of B−X. Both the B−X and D−X systems were also identified in low-temperature matrix isolation studies.[20,21]

Although these experimental studies characterized the X, B, and D states of XeF with good precision, they yielded no information about the third ion-pair state, C ($^3/_2$). Both the simple and the elaborate theoretical considerations indicated that this state lay at about the same energy as B, with its internuclear distance somewhat smaller.[7−10] In fact the most extensive computations placed the C state somewhat above B (and thus supported the adopted alphabetic labels for these states). Yet studies of relative emission intensities from the B and C states conducted at SRI[22] and Kansas State[23,24] indicated that the C state lay at least 600 cm^{-1} below B. The issue was more or less settled by Helm et al., who directly detected the weak C ← X transition in a transient laser-excitation experiment.[25] Their analysis of the vibrational structure in the C ← X spectrum placed the C state at T_e = 28 023 cm^{-1}, or 788 cm^{-1} below B.

About the time of the Helm et al. work on the C state, we published preliminary results of a rotational analysis of the B−X system for the single isotopomer ^{136}Xe^{19}F.[26] The reported parameters were based on fits of just transitions having N < 41, because for higher N the lines deviated progressively from predicted positions. These deviations could be accommodated

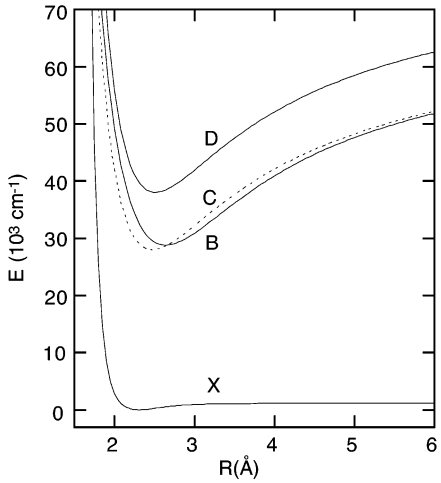

Figure 1. Potential diagram for XeF. Energies are relative to the minimum of the X state, which dissociates at 1175 cm^{-1}. The B and C (broken) states tend toward Xe$^+$ ($^2P_{3/2}$) + F$^-$ at 71 590 cm^{-1}, and D goes to Xe$^+$ ($^2P_{1/2}$) + F$^-$ at 82 130 cm^{-1}.

† Part of the special issue "Donald Setser Festschrift".

10.1021/jp0156221 CCC: $22.00
Published on Web 04/20/2002

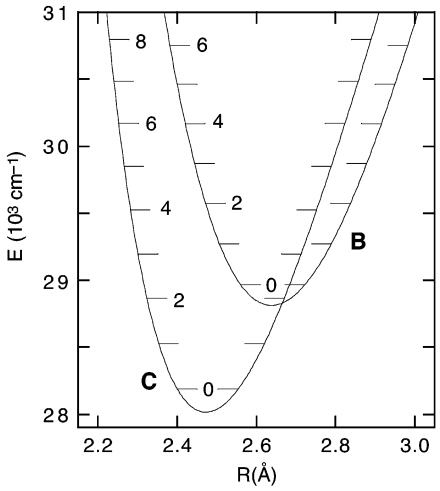

Figure 2. Expanded potential diagram for the low-v regions of the B and C states.

by adding additional terms to the rotational Hamiltonian for either the X state or the B state. In the former case, the effects would be due to anomalies associated with the unusual nature of the shallow X state (dissociation energy ~1200 cm^{-1}); in the latter they could be attributed to perturbative interactions with the C state. A subsequent study of the rotational structure in the D−X system of the same isotopomer[27] made it clear that the X state was behaving as predicted, and that therefore the second interpretation was the reason for the anomalies in the B−X spectrum. In the present work we have verified this interpretation by carrying out a deperturbation analysis of five bands in the B−X spectrum of ^{136}XeF. The results confirm the analysis of Helm et al.[25] and yield an improved characterization of both states in their low-v regions.

The situation for B−C perturbations is illustrated in Figure 2. The C state is located far enough below B that low v levels (v_B) in the B state lie just above levels $v_B + 2$ in the C state. Also, since the C state has a smaller internuclear distance R_e, its rotational constant is larger, permitting the (unperturbed) J levels of $v_C = v_B + 2$ to overhaul those of v_B in the B state from below. Levels of the same J and same e/f symmetry in the two states are mixed by the rotational Hamiltonian, with the effect being strongest where the two unperturbed levels coincide. The perturbation produces a mutual repulsion of the interacting levels, which is manifested as an upward shift in the frequencies of the B−X rotational lines for J below the coincidence level and a downward shift for levels above this point. Because the vibrational interval in the C state is larger than that in B, the mutually perturbing v levels in the two states move closer together with increasing v until they essentially coincide at $v_B = 4$. Thus the perturbed rotational region in the B state moves from quite high levels ($J > 70$) in $v_B = 0$ to $J \approx 0$ in $v_B = 4$. Levels $v_B = 5$ and higher are essentially unperturbed. (Levels v_B and $v_C = v_B + 1$ move into near proximity above $v_B \approx 15$, but levels this high are not detected in our emission spectra.)

In following sections of this work, we briefly summarize the experimental methods and theory of these perturbations and then describe the results obtained by fitting >1000 assigned lines in the 0−1, 1−1, 2−1, 3−1, and 4−1 bands to various models accounting for the perturbations. We report spectroscopic parameters for a model in which the C-state parameters are used to predict the Franck−Condon part of the perturbative interaction term in the Hamiltonian. This effectively reduces the perturbation to a single parameter that can be compared with predictions based on the pure precession model for the ion-pair states.

Experiments

The spectra were recorded photographically as described before.[26,27] The Tesla discharge sources contained 1−1.5 Torr SF_6, 2−3 Torr ^{136}Xe (Mound Laboratory, 95.2% isotopic purity), and 140−170 Torr Ar. Spectra were recorded in the 3300−3600 Å region and were calibrated with Fe lines from a microwave discharge Fe source. The spectrometer (1.5 m JY Model HR-1500) was equipped with a 3600-groove/mm holographic grating that gave a reciprocal dispersion of 1.35 Å/mm and a resolving power exceeding 2×10^5. The plates were read and processed using a modified microdensitometer/microcomputer system.[28] We estimate that sharp unblended spectral lines were measured with an absolute accuracy of ±0.03 cm^{-1}.

Theoretical Background

Both the D−X and B−X transitions display four strong branches in each $v'-v''$ band. These may be labeled R_e, P_e, R_f, and P_f, where R and P have their usual significance ($\Delta J = \pm 1$), and e and f are the symmetry labels.[15] The rotational energies in the $^2\Sigma^+$ ground state X may be represented

$$F_v''(\kappa'') = B_v''\kappa'' - D_v''\kappa''^2 + H_v''\kappa''^3 + L_v''\kappa''^4 + M_v''\kappa''^5 \quad (1)$$

where B_v'' is the rotational constant for level v in the X state, and D_v'', H_v'', etc. are the first through fourth centrifugal distortion constants. (Note that for the very anharmonic X state, the last two of these are indeed needed for the highest assigned rotational lines.) The rotational argument κ'' is different for the e and f levels,[29]

$$\kappa_e'' = N(N+1) + \alpha N$$
$$\kappa_f'' = N(N+1) - \alpha(N+1) \quad (2)$$

where N is the quantum number for rotation of the molecule about its center of mass and α is the constant which describes the spin-splitting between the two J levels that share a given N, $J_e = N + {}^1/_2$ and $J_f = N - {}^1/_2$. (α is related to the usual splitting constant γ by $\gamma = 2\alpha B_v''$.)

The ionic limit, $Xe^+(^2P) + F^-(^1S)$, gives rise to $^2\Pi$ and $^2\Sigma^+$ molecular states, with the $\Omega = {}^3/_2$ component of the $^2\Pi$ correlating with the lower $^2P_{3/2}$ limit. This component (C) remains purely Π in character, but the two $\Omega = {}^1/_2$ components (B and D) are strongly mixed states of both Σ and Π character and are best described using the Hund's case c expressions for $\Omega = {}^1/_2$ states,[15,30]

$$F_v'(\kappa') = B_v'\kappa' - D_v'\kappa'^2 \quad (3)$$

with κ again being different for the e and f levels,

$$\kappa_{e,f}' = J(J+1) - {}^1/_2 \mp \delta(J + {}^1/_2) \quad (4)$$

Under the assumption that only the aforementioned molecular states arising from $Xe^+(^2P) + F^-(^1S)$ are involved in the mixing

of the two $\Omega = {}^1/_2$ states,[30] the constants δ for the lower (B) and upper (D) states can be predicted,[15,30]

$$2\delta_B = 1 + \cos\theta - 2C_L \sin\theta$$
$$2\delta_D = 1 - \cos\theta + 2C_L \sin\theta \quad (5)$$

where

$$\cos\theta = (E_\Pi - E_\Sigma - A/2)/Y$$
$$\sin\theta = AC_L/Y \quad (6)$$

and

$$Y = [(E_\Pi - E_\Sigma - A/2)^2 + A^2C_L{}^2]^{1/2} \quad (7)$$

Here E_Σ and E_Π represent the unperturbed energies of the Σ and Π molecular states, A is the molecular fine structure constant, and $C_L = [L(L+1)]^{1/2}$ in this "pure precession" model.[31] (I.e., $C_L = \sqrt{2}$ here, since $L = 1$ for the Xe^+ ion.) More generally, C_L can be taken as an adjustable parameter to accommodate deficiencies in the model.[30] From the known spectroscopic energies (T_e) of these states, δ_B is predicted to be ~2 and $\delta_D \approx -1$, which means that the rotational level structure in the B state resembles that in a case a′ $^4\Sigma^-_{1/2}$ state, while that in D approximates an isolated $^2\Sigma^-$ state.[30] The values from analyzed rotational structure[16,19,26,27] are $\delta_B = 1.8$ and $\delta_D = -0.8$.

Perturbative interactions between the B and C states are induced by the rotational Hamiltonian. In the single-perturber approximation, the rotational levels of a given v_B level interact just with those of the nearest v level in C, which is $v_C = v_B + 2$ for the low v_B levels involved here (see Figure 2). The observed energies in the B state are then obtained by diagonalizing the resulting 2 × 2 matrix for $J_B = J_C$ (and the same e/f symmetry), yielding[29]

$$E = {}^1/_2(E_B + E_C) \pm {}^1/_2 Z \quad (8)$$

where

$$Z = [4|W|^2 + (E_B - E_C)^2]^{1/2} \quad (9)$$

Here E_B and E_C represent the unperturbed levels in the two states, and since the rotational levels of C overhaul those of B from below, the perturbed energies for B are obtained by taking the + sign in eq 8 for $E_C < E_B$ and the − sign for $E_C > E_B$. The perturbation element is given by[32,33]

$$W = W_{el}B_{BC}\,[J(J+1) - {}^3/_4]^{1/2} \quad (10)$$

where B_{BC} is an "interstate" rotational constant,

$$B_{BC} = \frac{h}{8\pi^2 c\mu}\langle v_B|R^{-2}|v_C\rangle \quad (11)$$

This yields a Franck−Condon-type dependence for the interaction, since the $\langle R^{-2}\rangle$ integral is different for each v_B. The electronic matrix element is

$$W_{el} = [J_a(J_a+1) - \Omega_B\Omega_C]^{1/2} \quad (12)$$

in pure precession in a case c basis.[33] Thus W_{el} is predicted to be $\sqrt{3}$ in this basis (since $J_a = {}^3/_2$ and the two Ω values are ${}^1/_2$ and ${}^3/_2$).

The case a basis that leads to eqs 5−7 is more flexible and potentially more informative. In the original $|\Lambda S\Sigma;\ \Omega JM\rangle$ set, the Σ state ($\Lambda = 0$, $\Sigma = {}^1/_2$) is coupled to the $\Pi_{3/2}$ state ($\Lambda = 1$, $\Sigma = {}^1/_2$) by a matrix element of form $C_L\hat{B}[J(J+1) - {}^3/_4]^{1/2}$, where $\hat{B}$ is the rotational operator that leads to elements such as that in eq 11, and C_L is as defined after eq 7. The $\Pi_{1/2}$ ($\Lambda = 1$, $\Sigma = -{}^1/_2$) and $\Pi_{3/2}$ components are coupled by an element that is the same except lacking the factor C_L. The two $\Omega = {}^1/_2$ components are coupled mainly by the spin−orbit element $AC_L/2$. Diagonalization of the 2 × 2 block for these components gives the B and D states, with B being expressed in terms of the original basis as[30]

$$|B\rangle = c|\Sigma\rangle - s|\Pi_{1/2}\rangle \quad (13)$$

The coefficients are related to the quantities in eqs 5−7 by $(c^2 - s^2) = \cos\theta$ and $2sc = \sin\theta$. [Hence $c = \cos(\theta/2)$ and $s = \sin(\theta/2)$.] This diagonalization yields for the matrix element coupling B and C,

$$H_{BC} = (s - cC_L)B_{BC}[J(J+1) - {}^3/_4]^{1/2} \quad (14)$$

from which, by comparison with eq 10, $W_{el} = (s - cC_L)$.

The predictions of eq 14 for W_{el} can be compared with that of eq 12 by considering eq 14 in the ionic dissociation limit. If we take $C_L = [L(L+1)]^{1/2} = \sqrt{2}$, we find $\cos\theta = {}^1/_3$ and $\sin\theta = -\sqrt{8/9}$, from which $s = -\sqrt{1/3}$ and $c = \sqrt{2/3}$. This gives $(s - cC_L) = -\sqrt{3}$ in eq 14, in agreement (apart from sign) with the case c result in eq 12. In the molecular binding region of internuclear distance R, we allow for deviation of C_L from the pure precession result and solve for C_L and A using the observed δ_B and energies of the three states.[30] The B and C potentials cross approximately at the minimum of the B state (Figure 2), at which R the D state lies very nearly 10^4 cm^{-1} higher. From these energies and $\delta_B = 1.83$ (see below), we obtain $C_L{}^2 = 1.53$ and $A = -7.2 \times 10^4$ cm^{-1}. These values yield $W_{el} = 1.58$, which is 9% smaller than the estimate from the case c basis.

If the two potential curves are known, the $\langle R^{-2}\rangle$ integrals in eq 11 can be evaluated using standard numerical methods to obtain the relevant one-dimensional wave functions.[34] In practice, a deperturbation analysis often involves one "dark" state that is not well known apart from the perturbation. That role is played by the C state in the present case, because the analysis of Helm et al.[25] is not sufficiently precise to permit reliable computation of these quantities. Thus, the primary goal of the analysis is the refinement of the spectroscopic parameters of the C state to yield a description of the perturbative interactions that is optimally consistent with eqs 8−11. In this analysis the quantity W_{el} is retained as an adjustable parameter and compared later with the predictions of eqs 12 and 14.

Results and Discussion

The v_B−1 B−X bands ($v_B = 0$−4) were selected for the present study, because the Franck−Condon factors predict all of these to be sufficiently intense to permit full assignment to high J.[16] Indeed, four of the five were included in our brief report,[26] and for most of these the assignments already extended beyond $N = 40$, even though the reported results were based on fitting only lines having $N < 41$, as already noted. Expansion of the assignments to still higher N was straightforward when the data were fitted in band-by-band fashion to a deperturbation model based on eqs 8−10. The final line list extended beyond $N = 65$ for most branches in most of the bands, and as high as

TABLE 1: Perturbation Parameters for B−C Interactions in $^{136}Xe^{19}F$ from 27-Parameter Nonlinear Fit of 1005 Assigned Lines in the 0−1, 1−1, 2−1, 3−1, and 4−1 Bands of the B−X System[a]

$v_B - v_C$	f[b]	g[b]
0−2	0.290(3)	$-4.1(5) \times 10^{-6}$
1−3	0.204(2)	$-1.0(4) \times 10^{-6}$
2−4	0.0903(9)	$4(2) \times 10^{-7}$
3−5	0.0060(6)	0[c]
4−6	0.074(2)	$-3.8(1.5) \times 10^{-6}$

C state: $T_e = T_{e,B} - 801.3(1.2)$; $\omega_e = 346.5(4)$; $\omega_e x_e = 2.22(3)$
$B_e = 0.165\ 90(14)$; $\alpha_e = 0.001\ 56(3)$
D_e[d] $= 1.524 \times 10^{-7}$; β_e[d] $= 1.0 \times 10^{-9}$

fit variance = 0.001 01 cm^{-2}

[a] Parameters not given here are presented in Table 2, as determined in final global analysis. [b] Fitted quantity, from eq 10, is $W' \equiv 2W_{el}B_{BC} = f + gJ(J+1)$; quantities in parentheses are 1σ errors. [c] Not statistically significant, so set to zero. [d] Fixed, using Dunham relations.[29]

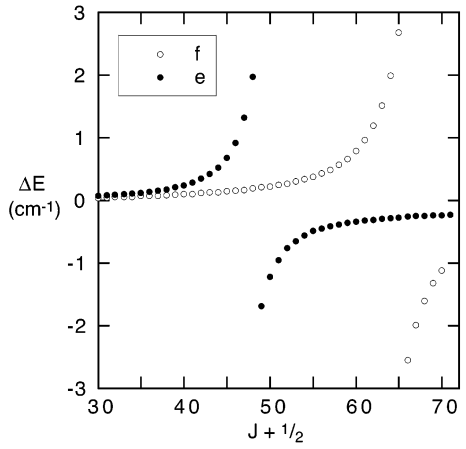

Figure 3. Energy deviations (perturbed−unperturbed) in level $v = 2$ of the B state from interactions with the C state.

$N = 81$ in the 0−1 band. The effect of the perturbation is strongest in the latter band, and because it occurs at high J, lines could not be assigned above the B/C crossover. The perturbation becomes progressively weaker in the 1−1 and 2−1 bands, and almost vanishes in the 3−1 band; and the B/C crossover J drops progressively with increasing v_B, in accord with expectations based on Figure 2. Accordingly, lines past the crossover could be assigned in these three bands. The crossover occurs very near $J = 0$ in $v_B = 4$ and is effectively weakened by the explicit J dependence in the perturbation matrix element (eq 10); still, the perturbation could be well determined from the least-squares fits for the 4−1 band.

In accord with eqs 3 and 4, the e and f levels of the B state are well separated at fairly low J and move progressively further apart, the splitting going as $\sim J$. In contrast the Ω-doubling in the C state should go as $\sim J^3$ and be much smaller than that in the B state for the observed range of J.[29−31] Numerical calculations based on the pure precession model behind eqs 5−7 indicate that this splitting is insignificant in the observed J range, and we have assumed in our analysis that the e and the f levels in the C state are unsplit and follow the same energy formula, namely eq 3 with $\kappa' = J(J+1)$. Since the e levels lie lower in the B state, this means that the perturbation occurs at significantly lower J in the e branches than in the f branches. This point is illustrated for $v_B = 2$ in Figure 3.

At the crossover point, both levels given by eq 8 are 50:50 mixtures of the B and C states. Since the C−X transition is more than an order of magnitude weaker than B−X,[25] the "B−X" lines will drop to about half their expected intensity at crossover, while "C−X" lines might become detectable there. The predicted weakening of the B−X lines was evident, with the lines for J near crossover sometimes being too weak to discern above background in the emission spectra. Model calculations predicted the "C" levels to be as much as one-third B character for only the 2−4 J levels closest to crossover. For such a short range of J, we concluded that we could not assign the C−X lines with confidence, because the spectra are congested and include overlapping lines from other bands in the regions in question. In an exception to this, we did doubly assign lines at the crossover in the 3−1 band, where the perturbation is so weak that the maximum shift is only ~0.2 cm^{-1}.

When the theory behind eqs 8−12 is implemented in matrix form, it is normally done tacitly or overtly in terms of rotationless ($J = 0$) basis sets. However, when energy levels are represented in terms of the usual expansion in κ in eq 1 or 3, the basis has already been effectively diagonalized in the centrifugal distortion (i.e., with respect to the off-diagonal *intrastate* $\langle v\ |R^{-2}|\ v'\rangle$ elements).[35] This "diagonalization" introduces a J dependence into the *interstate* $\langle v_B\ |R^{-2}|\ v_C\rangle$ matrix elements involved in the perturbations, which means that these elements must be evaluated specifically as functions of J in fitting the perturbed spectra to a realistic B/C mutual interaction model. Calculations showed that the $\langle v_B\ |R^{-2}|\ v_C\rangle$ matrix elements were, to a very good approximation, linear in κ, so they were represented this way in further computations.

The band-by-band deperturbation least-squares fits yielded estimates of $B_{v,C}$ and the energy differences $T_{v,B} - T_{v,C}$ for the mixed levels. These were used to obtain first estimates of T_e, ω_e, $\omega_e x_e$, B_e, and α_e for the C state in an all-bands fit. In the latter, the perturbation elements were initially represented in terms of two parameters for each v_B level: a constant and a coefficient of a term linear in κ,

$$W' \equiv 2\ W_{el}B_{BC} = f + gJ(J+1) \qquad (15)$$

Results for these 10 parameters (Table 1) reflect the Franck−Condon dependence of the perturbation.

If the model for the perturbative interaction is correct, the vibrational and rotational dependence of the B_{BC} constants in eqs 11 and 15 is entirely determined by the B and C potential curves, through the R^{-2} matrix elements. This means that the B_{BC} constants are effectively fixed by the other spectroscopic parameters for the two states, and the 10 adjustable parameters in Table 1 are reduced to the single parameter W_{el}. This maximally compact model was implemented in the final stage of the analysis, as follows. The B-state parameters were so well determined by the assigned lines that the B potential curve could be taken as known and constant for the determination of the R^{-2} matrix elements. The four C-state parameters (ω_e, $\omega_e x_e$, B_e, α_e) from the analysis of Table 1 were used to generate a reference RKR potential for the C state, which was then used to calculate the B_{BC} constants for a range of J. Each of the four spectroscopic parameters was then incremented slightly in turn, and the computations were repeated. From the results of these calculations, the matrix elements and their κ dependence were expressed as linear functions of the four parameters, for incorporation in the nonlinear fit. By this procedure the B_{BC} constants were tied to the other adjustable parameters without the computational inconvenience of having to iteratively refine the C potential, solve the Schrödinger equation, and compute the overlap elements within the nonlinear fit.[36] After a first pass, the reference potential for the C state was updated and the

TABLE 2: Nonlinear Deperturbation Analysis of the B−X System in $^{136}Xe^{19}F$[a]

parameter	B state	C state
T_e	28 811.67[b]	28 014.5[b]
ω_e	308.091(4)	345.08(23)
$\omega_e x_e$	1.4803(8)	2.100(25)
B_e	0.145 294(13)	0.165 416(33)
α_e	$6.747(9) \times 10^{-4}$	0.001 481(12)
D_e[c]	1.293×10^{-7}	1.520×10^{-7}
β_e[c]	1.72×10^{-9}	-4.6×10^{-10}
R_e (Å)	2.6383(1)	2.4726(2)

$$\delta_B = 1.827(3) + 0.0072(2)(v_B + {}^1/_2)$$

$$B_1'' = 0.181\,459(13); \quad D_1''\,[d] = 7.332(6) \times 10^{-7}; \quad \alpha_X = -0.035(3)[e]$$

$$W_{el} = 1.632(3)$$

$$\text{fit variance} = 0.001\,18\ \text{cm}^{-2}$$

[a] Units cm^{-1}. Interstate rotational constants B_{BC} for the perturbations were computed numerically from RKR potentials for the B and C states and were included in the optimization, as described in text. [b] Based on ref 26 for the X state. The fitted quantities were the energy of the B state relative to $v = 1$ in the X state, 28 498.117(5) cm^{-1}, and the energy of the C state relative to B, −797.2(5) cm^{-1}. [c] Determined in fit from other parameters, through Dunham relations.[29] [d] $H_1'' = -1.216 \times 10^{-11}$, $L_1'' = -4.39 \times 10^{-16}$, $M_1'' = -2.29 \times 10^{-20}$, units cm^{-1}, from ref 27. [e] An additional splitting term $\pm q[N(N+1)]^2$ was included for the e/f levels of $v_X = 1$, giving $q = 6.0(3) \times 10^{-9}$ cm^{-1}.

TABLE 3: $\langle v_B \mid R^{-2} \mid v_C \rangle$ Matrix Elements (Å^{-2}) in $^{136}Xe^{19}F$, as Calculated Using B and C Potentials Derived from Parameters Given in Table 2

$v_B - v_C$	$\langle v_B \mid R^{-2} \mid v_C \rangle_0$[a]	$10^7 d\langle R^{-2}\rangle/d\kappa$[b]
0−2	0.081 00	−1.43
1−3	0.060 56	2.11
2−4	0.027 04	4.65
3−5	−0.002 29	5.53
4−6	−0.023 03	5.23

[a] Calculated for rotationless potentials, $\kappa = 0$. [b] Derivative with respect to $\kappa = J(J+1)$. Note that because of the sign differences, the *magnitude* of the last two elements is actually decreasing with increasing κ.

procedure was repeated, with very little further change, indicating convergence. Results of this analysis are given in Table 2, and the computed R^{-2} matrix elements are presented in Table 3. The assigned lines and fit residuals are available as Table 4S (Supplementary Information).

Initially, this compact model yielded a 34% increase in the fit variance compared with that from the 27-parameter model. However, residuals analysis revealed several outliers, especially two weak lines in the P_f branch of the 4−1 band having residuals >0.2 cm^{-1}. Deletion of these dropped the variance by 10%, and further editing of the assignments led to another ∼15 deletions and additions, with a net reduction of 11 assigned lines, to yield the final data set of Table 4S. The latter was then used to obtain the results given in Tables 1 and 2.

The final variance from the compact model still exceeded that from the 27-parameter model by 17%. We conducted several additional fits in an attempt to identify the primary source of this increase. Allowance for R dependence in W_{el} dropped the variance by 7%; however, the resulting R dependence was much stronger than is considered reasonable. Wavenumber calibration errors were checked by incorporating parameters to correct selected band origins, but these showed only ∼4% improvement, supporting the absolute reliability of the measurements (which were taken from several different spectrograms). Addition of a scaling parameter for the B_{BC} values for selected bands gave a maximum improvement of 8% when applied for the 0−1 band. The magnitude of the correction was only 2.7% in this case, and it is conceivable that errors of this magnitude stem from the single-perturber approximation. In particular, the weakness of the perturbation for $v_B = 3$ is an especially sensitive locator for the C potential, and small changes in the absolute strength of the interaction could have a large relative effect for this level. In any event, the full set of residuals from the compact model of Table 2 well approximated a Gaussian distribution, with a maximum discrepancy of 0.10 cm^{-1} and only slight systematic effects in the individual bands.

Comparison of the results in Tables 1 and 2 reveals that the uncertainties of the C-state parameters are greatly reduced in the compact model, by as much as a factor of ∼4 for B_e. This indicates that the analysis is even more sensitive to the indirect Franck−Condon dependence of the R^{-2} matrix elements than to the direct dependence on the energy levels (i.e., from eqs 8 and 9). In particular, the greatly increased precision in B_e shows that the FC dependence is especially sensitive to the location of the C potential along the R axis (since R_e is directly determined by B_e). On the other hand, all five spectroscopic C-state parameters in Table 2 differ by more than 2σ from their estimates in Table 1. These results are all in good agreement with the much less precise estimates obtained by Helm et al.,[25] the most significant discrepancy being our 8.5 cm^{-1} smaller T_e value.[37] The fitted W_{el} is 6% below the case c estimate from eq 12 and just 3% above the case-*a*-based estimate derived after eq 14. The B-state parameters differ by small but statistically significant amounts from their counterparts from the earlier, low-J-restricted analysis,[26] which ignored the perturbation.

Conclusion

The 0−1, 1−1, 2−1, 3−1, and 4−1 bands in the B−X emission spectrum of $^{136}Xe^{19}F$ are analyzed by taking into account perturbations between the B and C ion-pair states. For these five B-state levels, the primary interactions are with the single levels $v_C = v_B + 2$. Nonlinear least-squares fits based on this single-perturber approximation yield results for the C state that are consistent with estimates from earlier work. The electronic matrix element for the perturbation is within 3% of expectations for Coriolis coupling of the B and C states. The slight deterioration in the quality of the fit for a model in which the Franck−Condon dependence of the perturbation is incorporated directly, as compared with one in which all perturbation elements are freely adjustable, could be due to limitations in the single-perturber approximation. This possibility is under continued investigation, as we also expand the assignments in an attempt to better describe the quite anomalous XeF ground state. The latter is chemically "bound" when viewed from the standpoint of its vibrational frequency (∼226 cm^{-1}), but not from the standpoint of its dissociation energy (∼1175 cm^{-1}).

The XeF molecule was discovered in the early 60s but first burst into prominence in 1975 as the lasant in a new excimer laser. Early in 1975, Setser enlisted the services of one of us (JT) in the effort to understand, through computational modeling, the structure in low-pressure (and mostly bound-free) XeF emission spectra.[38] A few months later, high-pressure spectra recorded at Sandia revealed clear discrete structure for both XeF and XeCl, and we turned our attention toward analysis of those spectra as a more profitable course for determining the unknown potential curves. Although interest in the XeF B → X laser and the later discovered[39] C → A laser has waned in recent years, some work continues in this area.[40,41] More generally, the electronic properties of XeF and its RgX kindred remain topics of study.[42−46] The present work on the detailed nature of the

interactions between the B and C states in XeF provides satisfying closure to an old problem.

Acknowledgment. We thank Katherine Johnson and Keith Luckett for help reading, calibrating, and processing some of the spectra from microdensitometer data to tracings and line lists.

Supporting Information Available: The assigned lines and fit residuals from the analysis of Table 2 are available in Table 4S, obtainable free of charge via the Internet at http://pubs.acs.org.

References and Notes

(1) Weeks, J. L.; Matheson, M. S. In *Noble Gas Compounds*; Hyman, H. L., Ed.; University of Chicago: Chicago, 1963; p 95.
(2) Morton, J. R.; Falconer, W. E. *J. Chem. Phys.* **1963**, *39*, 427.
(3) Kuznetsova, L. A.; Kuzyakov, Y. Y.; Shpanskii, V. A.; Khutoretskii, V. M. *Vestn. Mosk. University Ser. II Khim.* **1964**, *19*, 19.
(4) Velazco, J. E.; Setser, D. W. *J. Chem. Phys.* **1975**, *62*, 1990.
(5) Brau, C. A.; Ewing, J. J. *Appl. Phys. Lett.* **1975**, *27*, 435.
(6) Searles, S. K.; Hart, G. A. *Appl. Phys. Lett.* **1975**, *27*, 243.
(7) Ewing, J. J.; Brau, C. A. *Phys. Rev. A* **1975**, *12*, 129.
(8) Krauss, M.; Liu, B. *Chem. Phys. Lett.* **1976**, *44*, 257.
(9) Dunning, T. H., Jr.; Hay, P. J. *Appl. Phys. Lett.* **1976**, *28*, 649.
(10) Dunning, T. H., Jr.; Hay, P. J. *J. Chem. Phys.* **1978**, *69*, 134.
(11) Ault, E. R.; Bradford, R. S., Jr.; Bhaumik, M. L. *Appl. Phys. Lett.* **1975**, *27*, 413.
(12) Brau, C. A.; Ewing, J. J. *J. Chem. Phys.* **1975**, *63*, 4640.
(13) Liskow, D. H.; Schaefer, H. F., III.; Bagus, P. S.; Liu, B. *J. Am. Chem. Soc.* **1973**, *95*, 4056.
(14) Tellinghuisen, J.; Tisone, G. C.; Hoffman, J. M.; Hays, A. K. *J. Chem. Phys.* **1976**, *64*, 4796.
(15) Tellinghuisen, J.; Tellinghuisen, P. C.; Tisone, G. C.; Hoffman, J. M.; Hays, A. K. *J. Chem. Phys.* **1978**, *68*, 5177.
(16) Tellinghuisen, P. C.; Tellinghuisen, J.; Coxon, J. A.; Velazco, J. E.; Setser, D. W. *J. Chem. Phys.* **1978**, *68*, 5187.
(17) Velazco, J. E.; Kolts, J. H.; Setser, D. W.; Coxon, J. A. *Chem. Phys. Lett.* **1977**, *46*, 99.
(18) Smith, A. L.; Kobrinsky, P. C. *J. Mol. Spectrosc.* **1978**, *69*, 1.
(19) Monts, D. L.; Ziurys, L. M.; Beck, S. M.; Liverman, M. G.; Smalley, R. E. *J. Chem. Phys.* **1979**, *71*, 4057.
(20) Goodman, J.; Brus, L. E. *J. Chem. Phys.* **1976**, *65*, 3808.
(21) Ault, B. S.; Andrews, L. *J. Chem. Phys.* **1976**, *65*, 4192.
(22) Kligler, D.; Nakano, H. H.; Huestis, D. L.; Bischel, W. K.; Hill, R. M.; Rhodes, C. K. *Appl. Phys. Lett.* **1978**, *33*, 39.
(23) Brashears, H. C., Jr.; Setser, D. W. *Appl. Phys. Lett.* **1978**, *33*, 821.
(24) Brashears, H. C., Jr.; Setser, D. W. *J. Phys. Chem.* **1980**, *84*, 224.
(25) Helm, H.; Huestis, D. L.; Dyer, M. J.; Lorents, D. C. *J. Chem. Phys.* **1983**, *79*, 3220.
(26) Tellinghuisen, P. C.; Tellinghuisen, J. *Appl. Phys. Lett.* **1983**, *43*, 898.
(27) Johnson, K.; Tellinghuisen, J. *Chem. Phys. Lett.* **1994**, *228*, 363.
(28) Tellinghuisen, P. C.; Guo, B.; Chakraborty, D. K.; Tellinghuisen, J. *J. Mol. Spectrosc.* **1988**, *128*, 268.
(29) Herzberg, G. *Spectra of Diatomic Molecules*; D. Van Nostrand Reinhold: Princeton, NJ, 1950.
(30) Kopp, I.; Hougen, J. T. *Can. J. Phys.* **1967**, *45*, 2581.
(31) Van Vleck, J. H. *Phys. Rev.* **1929**, *33*, 467.
(32) Hougen, J. T. *The Calculation of Rotational Energy Levels and Rotational Line Intensities in Diatomic Molecules*; NBS Monograph 115; National Bureau of Standards: Washington, DC, 1970.
(33) Bussieres, D.; Hoy, A. R. *Can. J. Phys.* **1984**, *62*, 1941.
(34) Tellinghuisen, J. *Adv. Chem. Phys.* **1985**, *60*, 299.
(35) Lefebvre-Brion, H.; Field, R. W. *Perturbations in the Spectra of Diatomic Molecules* **1986**, Academic Press: Orlando, Florida.
(36) Brown, S. W.; Dowd, C. J., Jr.; Tellinghuisen, J. *J. Mol. Spectrosc.* **1988**, *132*, 178.
(37) The vibrational parameters of ref 25 were obtained from measurements on a natural abundance mix of XeF isotopomers rather than the single species $^{136}Xe^{19}F$ studied here. Allowance for the isotope effect for "average-mass" $^{131.3}XeF$ vs ^{136}XeF ($\sim$1 cm^{-1}) brings the present estimate for ω_e into near-perfect agreement with the 346 cm^{-1} obtained in ref 25.
(38) Tellinghuisen, J. *Pure Appl. Phys.* **1982**, *43*−*3*, 251.
(39) Bischel, W. K.; Nakano, H. H.; Eckstrom, D. J.; Hill, R. M.; Huestis, D. L.; Lorents, D. C. *Appl. Phys. Lett.* **1979**, *34*, 565.
(40) Mikheev, L. D.; Stavrovskii, D. B.; Zuev, V. S. *J. Russ. Laser Res.* **1995**, *16*, 427.
(41) Malinovskii, G. Y.; Mamaev, S. B.; Mikhjeev, L. D.; Moskalev, T. Y.; Sentis, M. L.; Cheremiskin, V. I.; Yalovoi, V. I. *Quantum Electron.* **2001**, *31*, 617.
(42) Zerza, G.; Sliwinski, G.; Schwentner, N.; Hoffman, G. J.; Imre. D. G.; Apkarian, V. A. *J. Chem. Phys.* **1993**, *99*, 8414.
(43) Lo, G.; Setser, D. W. *J. Chem. Phys.* **1994**, *100*, 5432.
(44) Pavlenko, V. S.; Nalivaiko, S. E.; Egorov, V. G.; Rzhevsky, O. S.; Gordon, E. B. *Chem. Phys. Lett.* **1996**, *259*, 204.
(45) Schröder, D.; Harvey, J. N.; Aschi, M.; Schwarz, H. *J. Chem. Phys.* **1998**, *108*, 8446.
(46) Hoffman, G. J.; Colletto, M. *J. Chem. Phys.* **2001**, *114*, 2219.